Journal of Thermal Analysis and Calorimetry, Vol. 79 (2005) 545–554

WORLD OF NANOSTRUCTURES – NANOTECHNOLOGY SURFACE PROPERTIES OF CHOSEN NANOMATERIALS Determined by adsorption, Q-TG, AFM and SEM methods

P. Staszczuk[*]

Department of Physicochemistry of Solid Surface, Chemistry Faculty, Maria Curie-Skłodowska University, Maria Curie-Skłodowska Sq. 3, 20-031 Lublin, Poland

The paper presents the basic information on nanotechnology and the recent results of studies of physicochemical properties of chosen nanomaterial surfaces (montmorillonites, carbon nanotubes, smart surfaces) by means of complex measuring methods. Physicochemical properties of nanomaterial surfaces by means of the special thermogravimetry Q-TG, sorptometry, porosimetry, atomic force microscopy (AFM) and scanning electron micrograph (SEM) methods were investigated. A numerical and analytical procedure for the evaluation of total heterogeneous properties (desorption energy distribution and pore-size distribution functions) on the basis of liquid thermodesorption from the sample surfaces under the quasi-equilibrium conditions and sorptometry techniques are presented. The evaluation of the fractal dimensions of nanotubes using the sorptometry, porosimetry, thermogravimetry Q-TG and AFM data are presented. The comparison of fractal coefficients calculated based on them with the results from Q-TG, sorptometry, porosimetry and AFM gave good agreement.

Keywords: *nanomaterials, nanotechnology, Q-DTG, Q-TG, thermogravimetry, total (energetical and geometrical) heterogeneity*

Introduction

At present main interest of interdisciplinary studies are focused on development of theoretical and experimental papers concerning nanomaterials and their practical applications [1]. Interest in the nanoworld is enormous and nanotechnology is at present the most dynamically developing discipline of science and technology e.g. over 30 nanotechnological research centres exist at universities. Nanotechnology deals with production and studies of properties of very small objects which can be applied in practice in future [2]. The nanotechnology term was given by Norio Taniguchi in 1974 to determine processing with the accuracy smaller that 1 μm but its quick development and diminution of objects in practice as well as manipulation of molecules on a small scale were predicted by Richard Feynman in 1957 [3].

The subject of nanotechnology is search and synthesis, characteristics, making use and practical application of new materials of advanced technology which possesses the sizes of nanometers. Such nanostructures are the bridge between individual atoms and molecules where quantum mechanics laws are applied and vast volume phase in which most properties result from collective behaviour of billion atoms. Individual nanostructures are clusters, nanomolecules, nanocrystals so called quantum points nanowires and nanotubes which possess orderly structures and they can be large molecules in single nanostructures [4]. Quantum size and shape of nanomolecules affect mechanical, chemical, electrical properties, nuclear-electronic, electric-optical and dynamic levels of structure. That promotes disclosure of new, unique physicochemical phenomena and more profitable than large structures such as quantitative differences in properties compared with the volume phase. This leads to possible control of action and application of nanostructures.

Nanotechnology must satisfy three criteria:

- Studied structures should have at least one size not larger than 100 nm. Thus nanotechnology is not technology in many cases.
- In the nanomaterial process production physicochemical properties should be controllable.
- There must be a possibility of building larger objects from the produced advanced materials.

The modern nanotechnology devices are scanning microscopes, mainly scanning tunnel microscope and atomic force microscope. Using these apparatus it is possible to obtain pictures of even single atoms and their dislocation on the surface.

Nanomaterials can be obtained using the methods from top to bottom and from bottom to top. The from top to bottom method consists in modelling of the surface by addition or removal of some amount of substance. In this way there are formed self-contained systems of the paths slightly broader than 100 nm.

* piotr@hermes.umcs.lublin.pl

1388-6150/$20.00
© 2005 Akadémiai Kiadó, Budapest
Akadémiai Kiadó, Budapest, Hungary
Springer, Dordrecht, The Netherlands

Table 1 Typical nanostructures given in [5]

Nanostructure	Size	Materials
clusters, nanocrystals, quantum dots	radius: 1–10 nm	insulators, semiconductors, metals, magnetic materials
other nanoparticles	radius: 1–100 nm	ceramic oxides
nanobiomaterials, photosynthetic reaction center	radius: 5–10 nm	membrane protein
nanowires	diameter: 1–100 nm	metals, semiconductors, oxides, sulphides, nitrides
nanotubes	diameter: 1–100 nm	carbon, layered chalcogenides
nanobiorods	diameter: 5 nm	DANN
2D arrays of nanoparticles	area: several nm^2–μm^2	metals, semiconductors, magnetic materials
surfaces and thin films	thickness: 1–1000 nm	insulators, semiconductors, metals, DNA
3D superlattices of nanoparticles	radius: several nm	metals, semiconductors, magnetic materials

However, in the from bottom to top method self-arrangement in formation of large structures is used. Under suitable conditions atoms or molecules form orderly systems spontaneously. In this way nanotubes are formed. The survey of typical nanostructures and their size are given in Table 1.

So far, advanced materials have found some application in practice. Fullerenes of a 1 nm diameter prepared for the first time in 1985 can be used as superconductors [6]. Carbon nanotubes discovered in 1991 were used in 1998 to build diode transistors, transmitters, logical gates but in 2003 in France to produce indestructible tights [7]. Moreover, they can be used as superconductors [8]. In 1999 single organic molecules and intersecting nanowires were used as catalysts for production of petrol. Non-magnetic layers of a thickness smaller than 1 nm placed between magnetic layers form computer hard discs of very large sensitivity and capacity. Drugs placed in lipid bags of a 100 nm diameter act longer because they circulate longer in the blood circulatory system. The biological tests for the presence and activity of searched substances are quicker, more sensitive and elastic when nanomolecules are used as markers [9]. Crystalline nanopowders improve properties of materials like chemical, mechanical, optical and magnetic ones. Harder ceramic materials, solar filters and catalysts used in the environmental protection are obtained. It is believed that in the near future microscopic robots will revolutionize the industrial production [10–12] and will be used in the interplanetary travels [13].

Studies of typical nanomaterials (soil mineral components adsorbents, silica gels with deposited proteins – so called smart surfaces, latexes, synthetic zeolites modified by ions, MCM-41 molecular sieves) were made earlier by author of this paper and published [14–20]. At present our research focuses on studies of surface properties (e.g. adsorption capacity), total heterogeneity (energetical and geometrical), surface layers as well as structure and phase transformation of fullerenes, carbon nanotubes, active carbons, semiconductors, high-temperature superconductors, modified zeolites and adsorbents with deposited proteins [21–28]. In this paper recent results are presented and discussed.

Experimental

Materials

The tested materials were Na- and La-montmorillonites from Lago Pellegrini (Argentina) [29, 30]. The substituted samples were obtained by saturation of the ion exchange capacities of the water-saturated clay samples with sodium and/or lanthanium chloride (0.5 M). Finally, the Na- and La-samples were air dried. Moreover, thermodesorption of liquids from natural zeolite–clinoptilolite and zeolite–mordenite (from Ukrainian Transcarpathian region) were made.

The carbon nanotube samples which were grown in a horizontal quartz tube reactor placed in a furnace by the reaction technique using xylene–ferrocene mixture by means of a method described in details in papers [26, 28] were examined. In our investigations of adsorbed liquids and surface porosity parameters of nanotubes we used carbon products obtained by two methods: DC electric arc generated between graphite electrodes and thermal decomposition of hydrocarbon vapour in the presence of catalyst (N-1 sample). This material was sonicated in the water/ethanol mixture for 30 min (N-2 sample). The fraction that precipitated on the bottom included nanotubes but there were mainly clusters. The N-3 sample was prepared by catalytic decomposition of xylene C_8H_{10} used as a carbon source and ferrocene $Fe(C_5H_5)_2$ as a catalyst precursor.

Bovine serum albumin (BSA, Fraction V, minimum 98%) was purchased from Sigma. Silica gel Davisil 653XWP (Z-300) was obtained from Supelco. Synthesis of ZS-300 (silica gel covered with chemically bonded triaminopropyltriethoxysilane) and ZB-300 (sil-

ica gel covered with BSA) samples were carried out using the method described in paper [27].

Spectral pulver carbon (powder, Elektrokarbon Topolcany N.P., Russia) was studied. We examined a Hg-1223 high-temperature sample prepared by a solid-state reaction technique using reagent-grade HgO, BaO, CaO and CuO powders by means of method described in paper [22]. A synthetic perovskite of chemical composition $LaCoO_3$ prepared by calcinations for 3 h at 1200°C [31] and fullerene – C70 (Sigma-Aldrich Chemie GmbH, Germany) were studied, too.

Apparatus

Thickness of the adsorbed liquid layers on the surface can be assessed by means of immersion mode of the solid samples. Adsorption of apolar (benzene and *n*-octane) and polar (water and *n*-butanol) liquid layers was measured using the derivatograph Q-1500 D (MOM, Hungary). The samples were saturated with liquid vapors in the vacuum dessicator at p/p_0=1.The Q-TG mass loss and Q-DTG differential mass loss curves were measured under the quasi-isothermal conditions in the temperature range 20–250°C at a heating rate of 6° min^{-1}.

Porosity properties e.g. specific surface areas, pore size distribution and pore volume were calculated from low-temperature nitrogen adsorption–desorption isotherms measured by means of the Sorptomat ASAP 2405 V1.01 with special program for preparation of the isotherms (Micrometrics Co., USA) and a Porosimeter 4000 (Carlo Erba Instruments). In order to characterize fully the structural changes caused by modification, atomic force microscopy (AFM) apparatus NanoScope III type (Digital Instruments, USA) and scanning electron micrographs were also obtained by means of the apparatus JSM-25 JOEL type. Surface coverage of samples by BSA was characterized by elementary analysis UV-Vis (Specord M 42, Carl Zeiss Jena) and infrared spectroscopy FTIR (PerkinElmer, Paragon, 1000).

Results

The Q-TG measurements

From the obtained experimental data of the liquid programmed thermodesorption under the quasi-isothermal conditions there were worked out the theoretical basis and methods of calculating the desorption energy distribution functions [32, 33] to estimate total heterogeneity of solid surfaces [34] and fractal coefficients [22]. The Q-TG mass loss and the Q-DTG differential mass loss curves of liquids as a function of temperature from the carbon nanotube surfaces are presented in Fig. 1. The characteristic inflections in the Q-DTG curves correspond to the individual stages of thermodesorption of the selected liquids from nanotube surfaces. It can be considered as a certain type of spectrum of thermodesorption process describing an energetic state of polar and apolar molecules on surfaces. The spectrum indicates long wide peaks with the minimum near 70°C (N-1/benzene), 115°C (N-2/*n*-octane) and 120°C (N-3/*n*-butanol) and a few other small peaks. It is shown from the data presented in Table 1 that the samples are highly sensitive to water vapour because the mechanism of molecule adsorption depends largely on the activated surface centres.

The energetic heterogeneity of materials is conditioned by the differences in topology of adsorption centres, dispersion of pore size and other factors. This paper presents the estimation of the energetic heterogeneity of carbon nanotubes making use of the results of the programmed thermodesorption of liquids from the solid surfaces. The final expression for determination of desorption energy distribution $\rho(E)$ can be expressed in the form [33, 34]:

$$\rho(E) = -\frac{\mathrm{d}\theta}{\mathrm{d}T}\frac{1}{T} \tag{1}$$

Equation (1) was used for the calculation of desorption energy distributions, $\rho(E)$, from the pores for each temperature T_i in the Q-TG and Q-DTG curves. The results for selected systems for *n*-butanol, water and benzene desorption from the surfaces within the temperature range T=50–180°C are presented in Fig. 2. The E_d values range 28–82 kJ mol^{-1} (benzene), 38–73 kJ mol^{-1} (*n*-butanol), 48–73 (*n*-octane) and 45–76 kJ mol^{-1} (water). In the case of benzene, the high value of desorption energy presented in Table 3 indicates great influence of the surface on adsorbed molecules. The thermodesorption of the above liquids shows that the investigated materials have non-polar surface properties.

The typical Gauss and bimodal shapes of the adsorption site distribution associated with the desorption of water from the surface may be observed for the modified N-2 sample as well as for the adsorption of *n*-butanol on N-1 and benzene on N-3 pure materials. However, changes in the distribution of adsorption sides which occur as a result of mechanical and chemical treatment appear somewhat complicated. The above treatment resulted in creation of low energy adsorption sites for the adsorbed molecules.

For aromatic hydrocarbons, a considerable increase of energy desorption value occurred in creation of high-energy adsorption sites for benzene molecules (Table 3). Figure 2 presents, for example, the distribution functions of the desorption energy for water on the N-2 material studied. This curve exhibits three maxima which suggests the presence of 3 types of active site for the sample under examination.

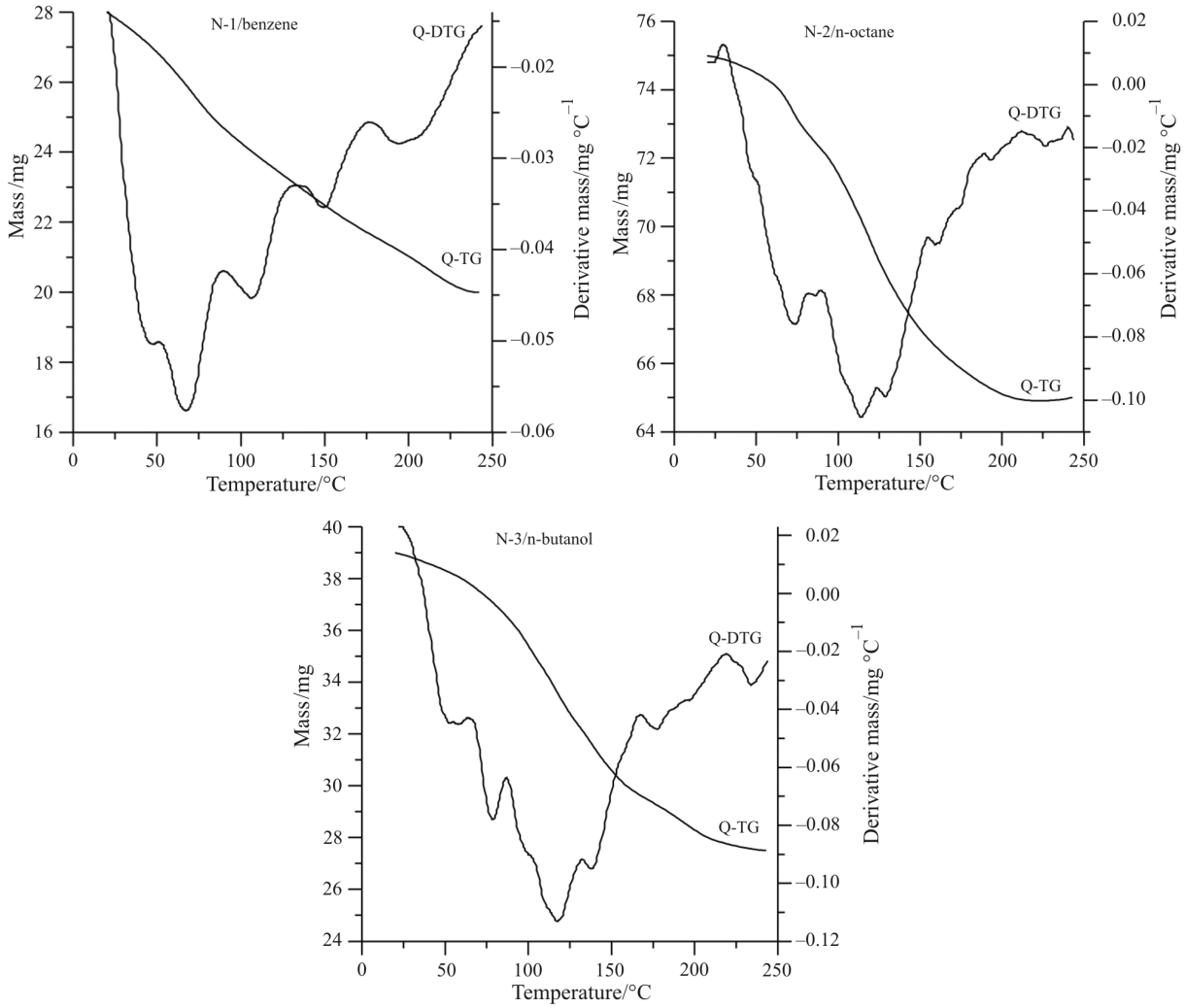

Fig. 1 The Q-TG and Q-DTG curves of benzene, *n*-octane and *n*-butanol thermodesorption from N-1, N-2 and N-3 samples, respectively

It follows, therefore, that mechanical and chemical modifications of N-2 nanotube sample causes not only a decrease in its porosity [26, 28] but also significant changes in its adsorption properties with respect to the adsorption of polar and apolar liquids (Table 2). The decrease in the specific surface area and pore volume of the modified N-2 surface may be attributed to the presence of the newly created pores and/or to an internal reorganization of the crystal network. The studied phenomenon is very complicated but the obtained results seem to be very promising for future investigations.

Structural properties of chosen advanced materials

From the sorptometry nitrogen adsorption–desorption data (Fig. 3) the specific surface area (*S*), total pore volume (*V*) and pore diameter (*D*) were calculated. These quantities were determined from the three Brunauer–Emmett–Teller (BET), Barrett–Joyer–Holenda (BJH) and Langmuir theories. The samples of silica gel (Z-300), gel after silanization (ZS-300) and the final product of modification with the protein BSA (ZB-300) deposited on the surface were sorptomatically studied.

Table 2 Adsorption capacity, *a*, and surface coverage degree, θ, of tested samples

Samples	water		*n*-butanol		benzene		*n*-octane	
	a/mmol g^{-1}	θ/mmol m^{-2}	*a*/mmol g^{-1}	θ/mmol m^{-2}	*a*/mmol g^{-1}	θ/mmol m^{-2}	*a*/mmol g^{-1}	θ/mmol m^{-2}
N-1	19.42	0.22	2.15	0.03	5.12	0.06	2.79	0.03
N-2	8.80	0.24	2.99	0.08	2.95	0.08	1.34	0.04
N-3	11.40	0.13	6.70	0.08	4.50	0.05	2.73	0.03

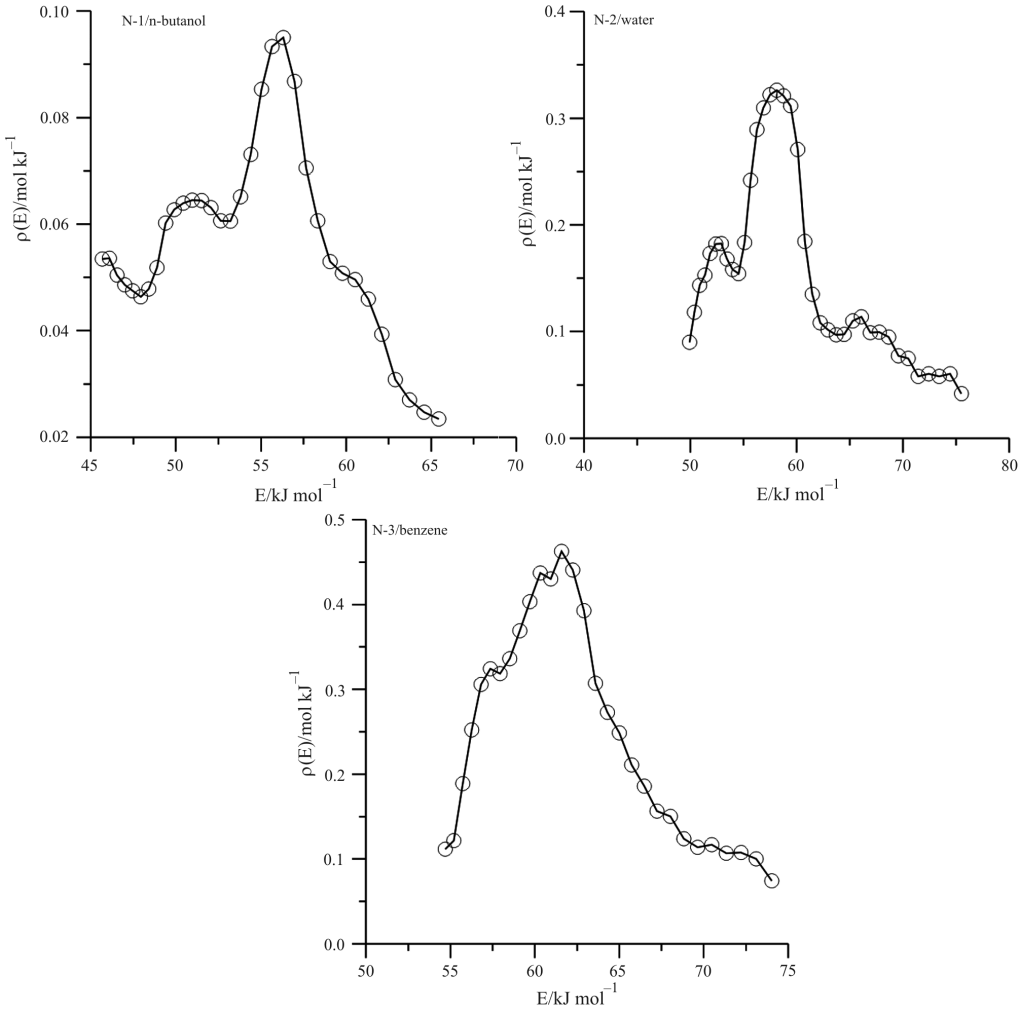

Fig. 2 Desorption energy distribution functions for N-1/*n*-butanol, N-2/water and N-3/benzene systems

The nitrogen adsorption–desorption isotherms for all analyzed samples presented in Fig. 3 have a shape of type IV according to the BET classification describing the capillary condensation phenomenon. This type of isotherm is connected with multimolecular adsorption layers formation and the hysteresis loop of capillary condensation with a steeply falling desorption branch was obtained in all cases. The obtained loops present type A of classification according to de Boer which indicates that capillaries have a shape of two-sided open, regular and irregular cylinders and prisms.

As follows from the data presented in Table 4 individual modifications affect significantly structure and adsorption properties of the surface of the studied samples. In the case of Z-300 a decrease in the nitrogen adsorption capacity is observed after modification with silane and BSA. For better illustration of porous structure of same sorbents, a diagram of pore-size distribution calculated from the desorption branch using the BJH method was made (Fig. 4). Analyzing the data in Table 4 and Fig. 4 an insignificant increase of pore diameter after silanization connected with the cross-linking increase is observed.

Table 3 The minimum, peak and maximium desorption energy values of liquids

Samples	Desorption energy/kJ mol^{-1}											
	benzene			*n*-butanol			*n*-octane			water		
	E_{dmin}	$E_{d(peak)}$	E_{dmax}	E_{dmin}	$E_{d(peak)}$	E_{dmax}	E_{dmin}	$E_{d(peak)}$	E_{dmax}	E_{dmin}	$E_{d(peak)}$	E_{dmax}
N-1	28	33	48	46	57	65	32	35	45	26	30	44
N-2	61	70	82	38	47	58	48	58	73	50	57	76
N-3	55	62	74	48	60	75	49	57	70	45	52	66

AFM and scanning electron micrograph photos

Figures 5–10 present, as example, the AFM pictures of surfaces of carbon nanotubes, carbon, fullerene and silica gel with the deposited BSA protein, respectively. From the AFM data fractal coefficients were calculated for the tested surfaces using the method described in [35] and commercial program in NanoScope III apparatus and presented in Table 5. Figure 11 shows the AFM photographs of the sample surfaces: pure Z-300 – I, after silanization – II and after modification with BSA – III. The photo (III) shows distinctly change of support surface porosity (coarseness) due to protein macromolecules addition. Figures 12–14 present scanning electron microraphs of the N-1, N-2 and N-3 carbon nanotube samples, respectively [26, 28]. There are additional illustration of the real advanced material surfaces.

Fractal dimension calculations

The many studies showed that some processes and structure difficult to be described by means of traditional Euclidean geometry can be precisely characterized using fractal geometry. While describing physical objects by means of fractal geometry, they are assumed the existence in the three-dimensional space. Fractals can be applied in many areas of science (topology, theory of multiplicity, Brownian motion), art, studies of nature and Galaxy distribution. Using fractals for description of real structures their most important properties are studied. Fractal geometry is frequently used to describe macroscopic objects. However, it can also be used for description of microstructure of solids of complex and disordered structure e.g. advanced materials, adsorbents, polymers, minerals. Recent studies have shown that using fractal dimensions enables determination of real sizes of pore radii from the data of programmed thermodesorption of liquid and calculations of the pore-size distribution functions [29].

The fractal dimensions were calculated from sorptometry data which is based on the theory by Frenkel, Halsey and Hill and also of Kisielev. The fractal dimensions D can be calculated from the following equations [22, 29]:

Table 4 Adsorption and structural parameters of the gel samples determined from the nitrogen adsorption isotherms

Samples	Z-300	ZS-300	ZB-300
$S_{BET}/m^2\ g^{-1}$	190.1	139.2	137.0
$V_{BJHads}/cm^3\ g^{-1}$	1.2	0.94	0.92
$V_{BJHdes}/cm^3\ g^{-1}$	1.2	0.93	0.81
R_{BET} /nm	25.1	26.6	23.6
R_{BJHdes} /nm	21.5	18.6	18.4

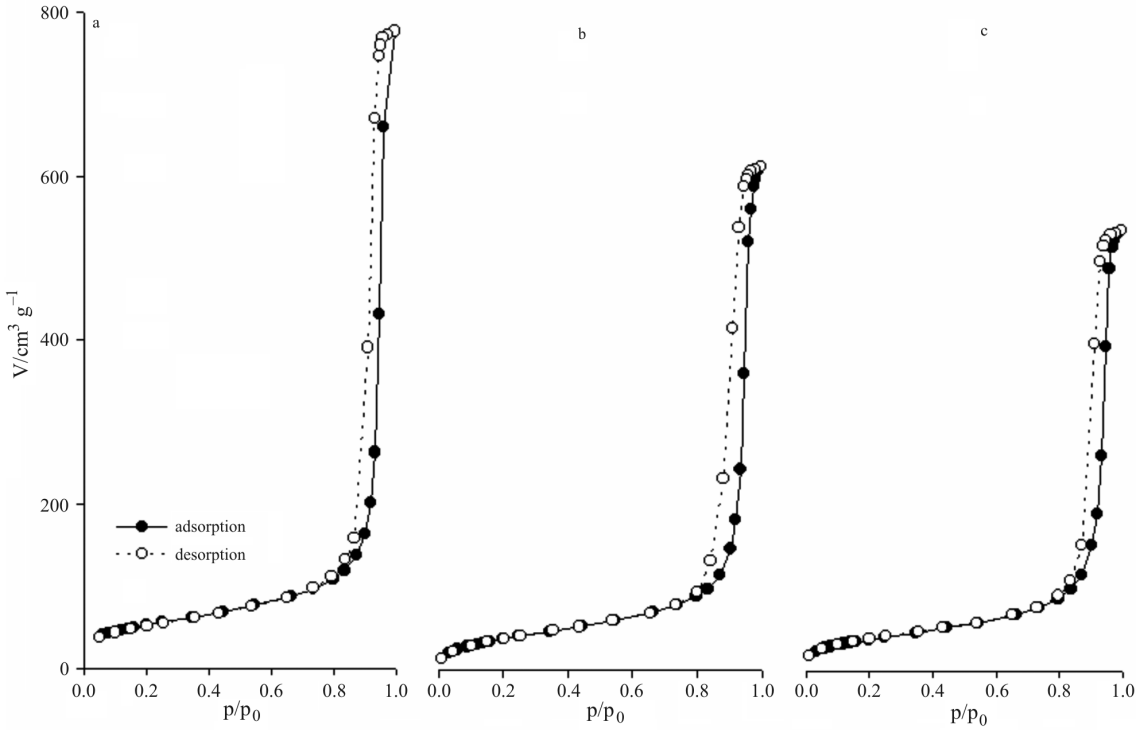

Fig. 3 Isotherms of nitrogen adsorption-desorption using commercial sorptomate apparatus from the samples: a – Z-300, b – ZS-300, c – ZB-300

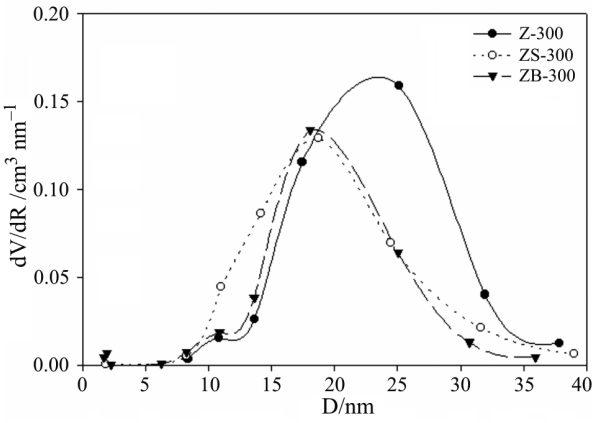

Fig. 4 Pore-size distribution functions of studied samples

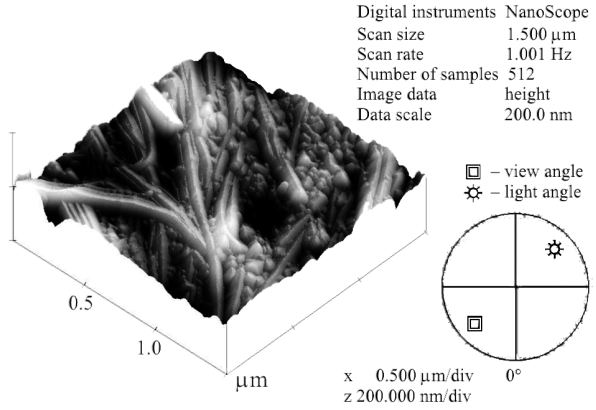

Fig. 5 AFM photo of N-1 carbon nanotube

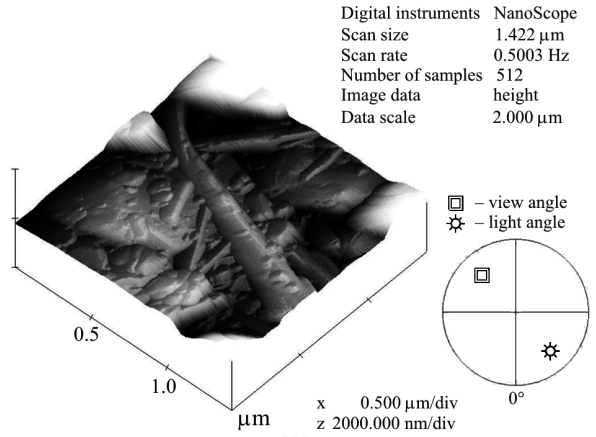

Fig. 6 AFM photo of N-2 carbon nanotube

$$D=2+n_f \quad (2)$$

$$D=3-\mathrm{d}[\ln a(x)]/\mathrm{d}[\ln(-\ln x)] \quad (3)$$

$$D=2+\mathrm{d}[\ln\int(-\ln x)\mathrm{d}a]/\mathrm{d}[\ln(-\ln x)] \quad (4)$$

$$\mathrm{d}V/\mathrm{d}r=A(r)\sim r^{(2-D)} \quad (5)$$

where n_f is a fractional part of the fractal, a is the size of adsorption, x is the segment of experimental isotherm, V and r are the volume and radius of pores. The function $A(r)$ is determined from the experimental data of the adsorption hysteresis.

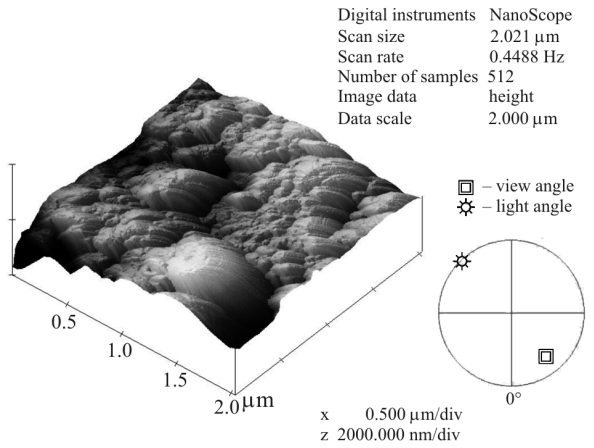

Fig. 7 AFM photo of N-3 carbon nanotube

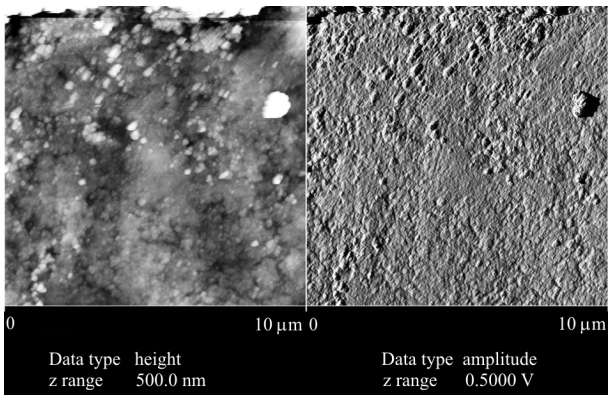

Fig. 8 AFM photo of active carbon

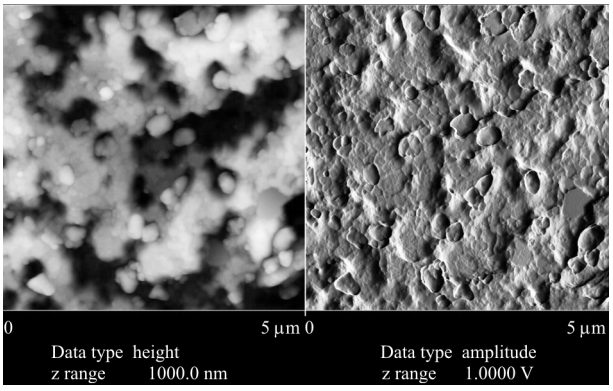

Fig. 9 AFM photo of fullerene

The Q-TG curves presented in Fig. 1 were transformed into the form of dependence $\ln[(m_0-m_1)S]$ as the function $\ln[(m_1-m_k)/d]$ where m is the initial mass of the sample; m_1 is the mass of the sample at a temperature T_i, m_k is the final mass of the sample, d is the liquid density and S is the specific surface area of the sample. The

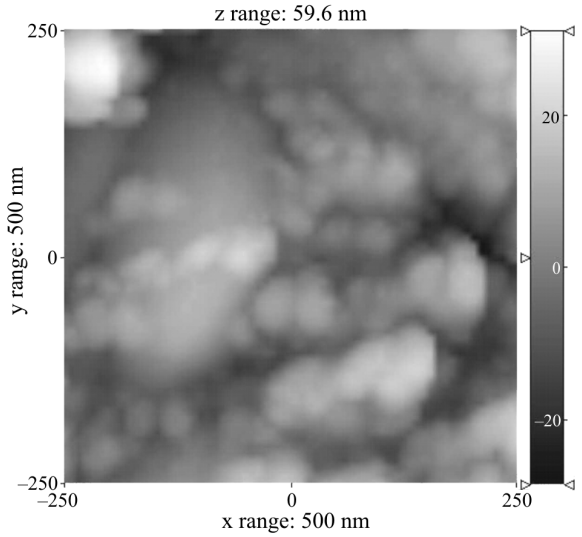

Fig. 10 AFM photo of smart surface

fractal dimension was calculated for this value of liquid mass loss by an analytical method from the slope of tangent C using the following equation [22, 29]:

$$D=(2+3n_f)/(1+n_f) \quad (6)$$

Fractal dimension from porosimetry data of sample studied were calculated from the following equation [36, 37]:

$$dV/dP \sim P^{D-4} \quad (7)$$

where V and P are the volume and pressure of mercury.

Fractal dimensions of samples can be calculated using a simple analytical method from the curves of the dependence of dV/dP as a function of P:

$$\log(dV/dP) \sim (D-4)\log P \quad (8)$$

Table 5 shows the fractal coefficients of chosen advanced materials calculated from the experimental data obtained using different and independent measuring methods. As follows from the data in Table 5, comparison of individual coefficients calculated using complex measuring techniques shows good agreement.

Fractal dimensions were used for calculation of the pore volume distribution functions in relation to their radii from Eq. [34]:

$$dV(r)/dr = 6.44 \cdot 10^{-3} r^{2-D} \quad (9)$$

where V is pore volume given from mass loss Q-TG curves, r – pore radius calculated from Eq. (10):

$$V=(r/r-t)^2 \quad (10)$$

where t is the thickness of the liquid films.

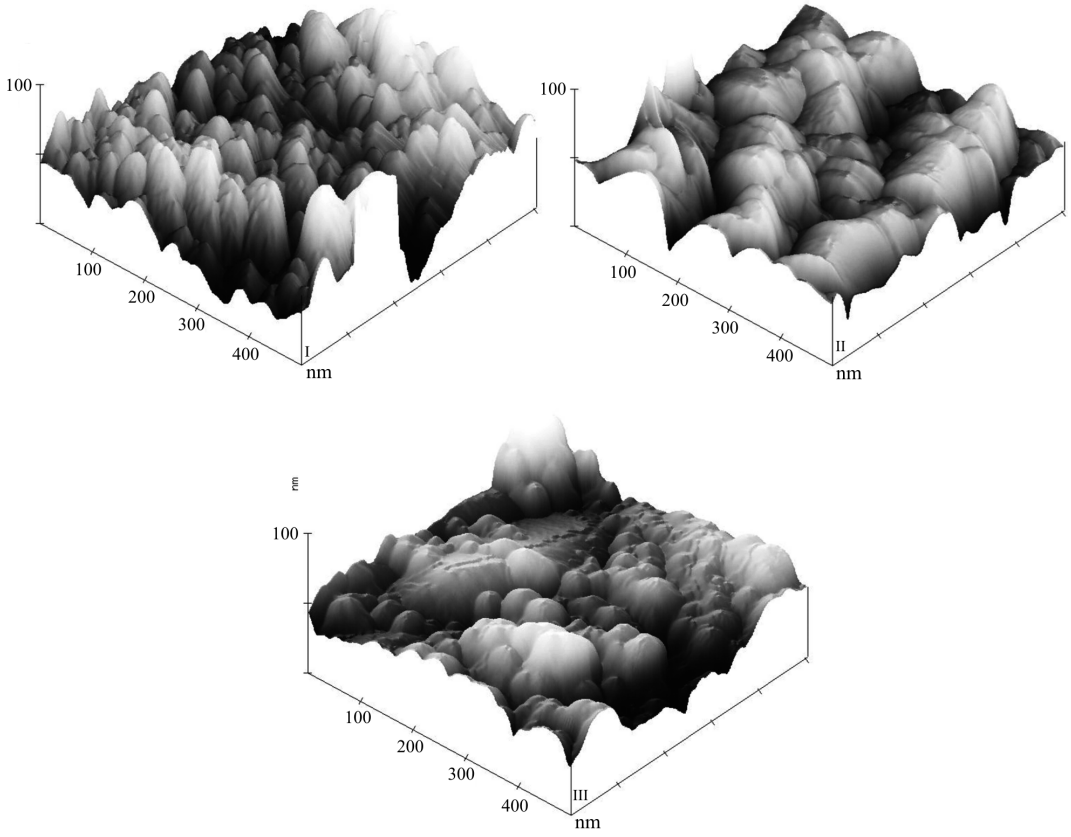

Fig. 11 AFM photographs of the sample surface: I– Z-300, II– ZS-300, III– ZB-300

Table 5 Fractal dimensions of chosen advanced material surfaces calculated on the basis of sorptometry, thermogravimetry Q-TG, porosimetry and AFM data

Samples	Sorptometry	Thermogravimetry Q-TG	Porosimetry	AFM
Na-montmorillonite [29]	2.49	2.45	2.88	
La-montmorillonite [29]	2.75	2.44	2.86	
Clynoptilolite [29]	2.61	2.47	2.90	
Mordenite [29]	2.59	2.45	2.87	
N-1 [26, 28]	2.49	2.50		2.33
N-2 [26, 28]	2.64	2.52		2.54
N-3 [26, 28]	2.54	2.49		2.34
Z-300 [27]	2.59			2.31
ZS-300 [27]	2.60			2.80
ZB-300 [27]	2.73			2.71
Carbon [38]	2.61			2.66
Superconductor [22]	2.60	2.49		
Perovskite [31]	2.27			2.53
Fullerene [38]	2.83			2.52

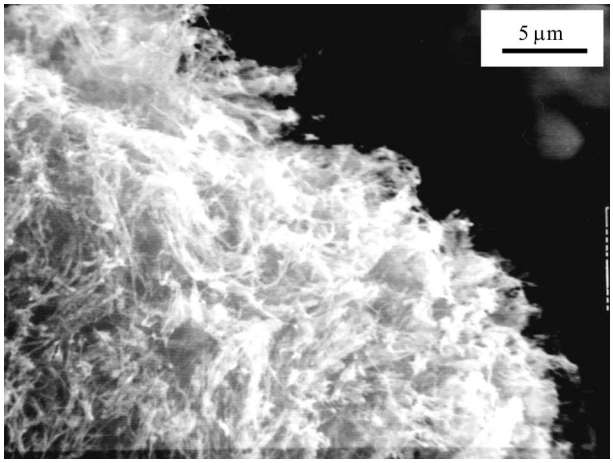

Fig. 12 Scanning electron micrograph of N-1 sample

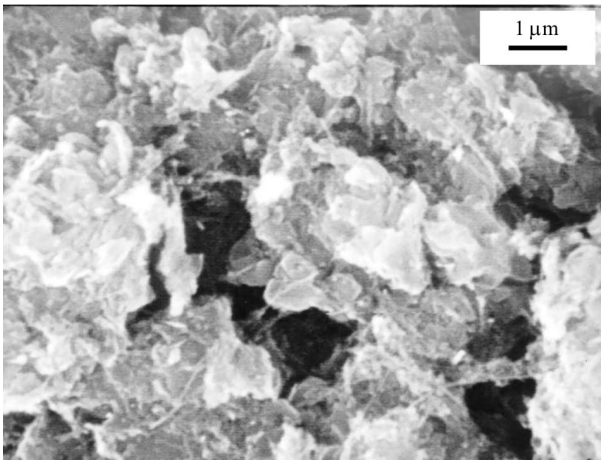

Fig. 13 Scanning electron micrograph of N-2 sample

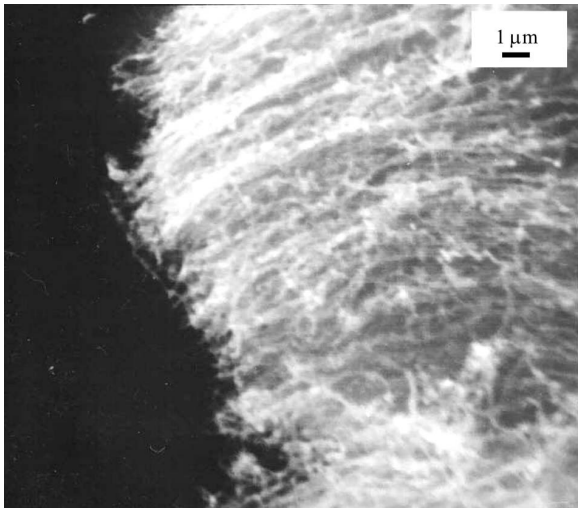

Fig. 14 Scanning electron micrograph of N-3 sample

Conclusions

Applications of thermogravimetry Q-TG for the investigations of adsorbed liquid layers and porosity parameters used for the quantitative characterisation of the energetic and geometrical (e.g. total) heterogeneities of typical advanced materials have been presented. The used method is very useful to investigate physicochemical properties of surface liquid films, adsorbate-adsorbent interactions and total surface heterogeneity. The thermodesorption process of liquids depends on the surface wetting phenomenon and surface properties of the solid surfaces. Comparison of the thermogravimetry and other data provide new information about the adsorption and pore structure of the studied materials. The N-1 and N-3 samples possess mesopores with homogeneous structure because the fractal dimensions

are close to 2.5. The modified N-2 sample was characterized by larger heterogeneity of the pores (fractal coefficients are higher than 2.5).

The fractal dimensions of studied materials surfaces using the Q-TG and independent techniques are presented. It is in good agreement with the results from sorptometry, porosimetry and AFM techniques and can be used for calculation of the pore-size distribution functions.

References

1 D. E. Nicolau, J. Phillimore, R. Cross and D. V. Nicolau, Microelectron. J., 31 (2000) 611.
2 G. Stix, Świat Nauki, 123 (2001) 24.
3 M. Roukes, Świat Nauki, 123 (2001) 40.
4 G. M. Whitesides and J. C. Love, Świat Nauki, 123 (2001) 31, 68.
5 J. Jortner and C. N. R. Rao, Pure Appl. Chem., 74 (2002) 1491.
6 M. S. Dresselhaus and G. Dresselhaus, Nanostruct. Mater., 9 (1997) 33.
7 C. M. Lieber, Świat Nauki, 123 (2001) 49.
8 M. Kociak, A. Yu. Kasumov, S. Gueron, B. Reulet, I. I. Khodos, Yu. B. Gorbatov, V. T. Volkov, L. Vaccarini and H. Bouchiat, Phys. Rev. Lett., 86 (2001) 2416.
9 A. P. Alivisatos, Świat Nauki, 123 (2001) 57.
10 K. E. Drexler, Świat Nauki, 123 (2001) 64.
11 R. E. Smalley, Świat Nauki, 123 (2001) 66.
12 S. Ashley, Świat Nauki, 123 (2001) 74.
13 G. P. Collins, Świat Nauki, 123 (2001) 76.
14 A. Waksmundzki, P. Staszczuk and E. Szymański, Pol. J. Soil Sci., 14 (1981) 25.
15 P. Staszczuk and A. Waksmundzki, Problemy Agrofizyki, Ossolineum Wrocław, 37 (1982) 1 (review).
16 A. Waksmundzki and P. Staszczuk, Zesz. Probl. Post. Nauk Roln., 220 (1983) 459.
17 E. Chibowski and P. Staszczuk, Clays Clay Miner., 36 (1988) 455.
18 P. Staszczuk, M. A. Cabrerizo-Vilchez and R. Hidalgo-Alvarez, Colloid. Polym. Sci., 271 (1993) 759.
19 P. Staszczuk, J. Thermal Anal., 48 (1997) 755.
20 P. Staszczuk, T. Danielkiewicz and J. Klinowski, Adsorpt. Sci. Technol., 18 (2000) 307.
21 P. Staszczuk, M. Majdan, T. Danielkiewicz and M. Matyjewicz, Prog. Colloid. Polym. Sci., 118 (2001) 100.
22 P. Staszczuk, D. Sternik and G. W. Chądzyński, J. Therm. Anal. Cal., 71 (2003) 173.
23 M. Majdan, M. Kowalska-Ternes, S. Pikus, P. Staszczuk, H. Skrzypek and E. Zięba, J. Mol. Struct., 649 (2003) 279.
24 V. Babiuk, P. Staszczuk, O. Bodak, Yu. Gorelenko, L. Romka and Y. Stadnyk, J. Alloys and Compd., 365 (2004) 21.
25 V. Kurpusyuk, N. Semus'o, R. Gładyszewski and P. Staszczuk, J. Alloys Compd., in press.
26 P. Staszczuk, M. Matyjewicz, E. Kowalska, J. Radomska, P. Byszewski and M. Kozłowski, Proceedings of SPIE, Nanotechnology, 5118 (2003) 245.
27 P. Staszczuk and D. Sternik, Proceedings of SPIE, Bioengineered and Bioinspired Systems, 5119 (2003) 210.
28 P. Staszczuk, M. Matyjewicz, E. Kowalska, J. Radomska, P. Byszewski and M. Kozłowski, Rev. Adv. Mater. Sci., 5 (2003) 34.
29 M. Matyjewicz and P. Staszczuk, J. Therm. Anal. Cal., 74 (2003) 413.
30 M. Matyjewicz, P. Staszczuk, J. C. Bazan and N. J. Garcia, Ann. Pol. Chem. Soc., 2 (2003) 659.
31 D. Sternik, P. Staszczuk, G. W. Chądzyński and B. Kucharczyk, Ann. Pol. Chem. Soc., 2 (2003) 688.
32 V. I. Bogillo and P. Staszczuk, J. Therm. Anal. Cal., 55 (1999) 493.
33 P. Staszczuk, D. Sternik and V. V. Kutarov, J. Therm. Anal. Cal., 69 (2002) 23.
34 P. Staszczuk, V. V. Kutarov and M. Płanda, J. Therm. Anal. Cal., 71 (2003) 445.
35 N. Almqvist, Surf. Sci., 355 (1996) 221.
36 W. I. Frisen and R. J. Mikula, J. Colloid Interface Sci., 120 (1987) 263.
37 S. P. Rigby, R. S. Fletcher and S. N. Riley, J. Colloid. Interface. Sci., 240 (2001) 190.
38 P. Staszczuk, Ann. Pol. Chem. Soc., 2 (2003) 677.